Available online at www.sciencedirect.com
SCIENCE DIRECT
Polymer 47 (2006) 4238–4244
polymer
www.elsevier.com/locate/polymer

# Transport in sulfonated poly(phenylene)s: Proton conductivity, permeability, and the state of water

Michael A. Hickner, Cy H. Fujimoto, Chris J. Cornelius *

*Sandia National Laboratories, Chemical and Biological Systems Department, P.O. Box 5800, MS 0734, Albuquerque, NM 87185-0734, USA*

Available online 18 April 2006

**Abstract**

The transport properties of a series of sulfonated poly(phenylene)s were found to strongly correlate to the ion exchange capacity of the polymer. Sulfonated poly(phenylene) membranes have shown promise as proton exchange membranes for fuel cells. In general, these materials have minimal methanol and glucose crossover while maintaining high proton conductivity, which is necessary for efficient operation of fuel cells powered by liquid fuels. Proton conductivity in addition to methanol and glucose permeability were compared to Nafion as a function of ion exchange capacity. It was found that the transport in Nafion membranes was much higher than that in the sulfonated poly(phenylene)s for a given ion exchange capacity. Water content and its absorbed state within membranes were elucidated by differential scanning calorimetry in order to provide insight as to how the transport properties varied between the materials studied. The domain morphology of these ionomers was imaged with transmission electron microscopy in order to contrast the morphological differences between Nafion and the sulfonated poly(phenylene) series.


*Keywords:* Fuel cell; Proton exchange membrane; State of water

## 1. Introduction

Selective transport through thin polymer films is desired for a wide range of applications such as water purification, dialysis, filtration, pervaporation, sensors, and fuel cells [1–8]. The presence of water within these materials can cause plasticization leading to a reduction in the glass transition temperature ($T_g$) and crystallinity resulting in a change in mass transport which is influenced by the concentration of water that is sorbed [9–11]. Water that sorbes into a polymer exists as bound water (through hydrogen bonding and dispersion forces), unbound water that is free to move via convective and normal diffusion, and weakly bound water that has intermediate properties between bound and unbound water [12]. For example, water binding has been observed using infrared spectroscopy in Nafion by measuring a wave number shift in sulfonic acid groups [13]. In a study utilizing positron annihilation lifetime spectroscopy, the water domain size increased with increasing water content for polyvinyl alcohol, and salt rejection and water transport were affected when water caused a depression in the $T_g$ of cellulose acetate as elucidated with dynamic scanning calorimetry (DSC) [14,15]. The measurement of bound and unbound water in polymers is not a new concept, but elucidating its relationship with structure and transport is necessary for creating new proton exchange membrane (PEM) materials and controlling their transport properties, which is important for liquid fed fuel cells [16–20].

This paper seeks to strengthen the correlation between the state of absorbed water in the membrane and the membrane's transport properties as it pertains to proton conductivity and permeability of methanol and glucose. Several PEMs for hydrogen, methanol, and glucose fuel cells are being investigated as an alternative to Nafion with the goal of minimizing fuel crossover (or membrane permeability) while simultaneously possessing sufficient proton conductivity [21–23]. However, increasing proton conductivity leads to a simultaneous increase in water uptake, which may negatively impact fuel crossover. A study of the role of mass transport as a function of increasing sulfonation level (or ion exchange capacity) within a homologous series of sulfonated poly(phenylene)s (SDAPP) will provide insight into the role of water content and its effect on transport and physical properties, which is necessary for designing a PEM for hydrogen and methanol fuel cells [24].

* Corresponding author.

0032-3861/$ - see front matter © 2006 Published by Elsevier Ltd.
doi:10.1016/j.polymer.2006.02.034

## 2. Experimental

### 2.1. Membrane synthesis, casting, and conversion

The synthesis and physical properties of the unsulfonated Diels–Alder poly(phenylene) and its sulfonation to form high molecular weight SDAPP ionomer is reported elsewhere [24]. Robust films of SDAPP in the salt form with thicknesses on the order of 50–100 μm were cast in a specially designed casting dish with a flat glass bottom from a solution of DMAC and SDAPP (5 wt% solids). Solvent was removed by drying under full vacuum for 24 h at ambient temperature followed by 4 h at 60 °C, 4 h at 80 °C, and 2 h at 100 °C to yield clear, homogeneous films. SDAPP films were converted from their salt form to their acid form by immersion in boiling 1 M $H_2SO_4$ for 2 h. Excess $H_2SO_4$ was removed from the films by rinsing them in boiling water for 2 h followed by additional water rinses to remove any remaining acid. All film rinses were performed in 18 MΩ water and all SDAPP films were stored in 18 MΩ water prior to testing.

Nafion 117 films used in this study were purchased in the sodium salt form from Aldrich. The membranes were treated by the standard method of boiling in 3 wt% $H_2O_2$ to remove trace organics and then converted to the acid form by boiling in 1 M $H_2SO_4$ [25]. Excess $H_2SO_4$ was removed from the films by rinsing them in boiling water for 2 h that was followed by additional water rinses to remove any remaining free acid. All membrane rinses were performed in 18 MΩ water and membranes stored in 18 MΩ water prior to testing.

### 2.2. Water uptake, ion exchange capacity, and hydration number

Water uptake on a mass basis was determined gravimetrically. The acid form of the film samples was allowed to equilibrate at room temperature in 18 MΩ water. They were quickly removed from the water, blotted dry to remove surface water, and immediately weighed to determine the wet mass of the film ($m_{wet}$). The films were then dried under full vacuum at 120 °C for 24 h then weighed again to determine the dry mass of the film ($m_{dry}$). This temperature was below their degradation temperature as determined in pervious studies [24]. Complete water removal was confirmed by sequential mass measurements during drying. Water uptake was calculated by the following equation.

$$\text{Water uptake} = \left[\frac{m_{wet} - m_{dry}}{m_{dry}}\right] \times 100\% \quad (1)$$

The IEC of the membrane samples was determined by titration of the proton form of the polymer as detailed in Ref. [24].

The hydration number (λ) is determined from the IEC of the membrane, the dry mass of the sample, the mass of water absorbed ($m_{H_2O}$ = wet film − dry film mass), and $MW_{H_2O}$ is the molecular weight of water as given in Eq. (2).

$$\lambda = \frac{m_{H_2O}/\mathrm{MW}_{H_2O}}{m_{dry}\mathrm{IEC}} \times 1000 \quad (2)$$

### 2.3. Proton conductivity

Proton conductivity was measured by electrochemical impedance spectroscopy (EIS) in a 'window cell' design [24,26] All membranes were immersed in liquid water at the temperature of interest during the EIS measurement.

### 2.4. Methanol and glucose permeation

Methanol permeability was determined using a membrane-separated diffusion cell as shown in Fig. 1(a).

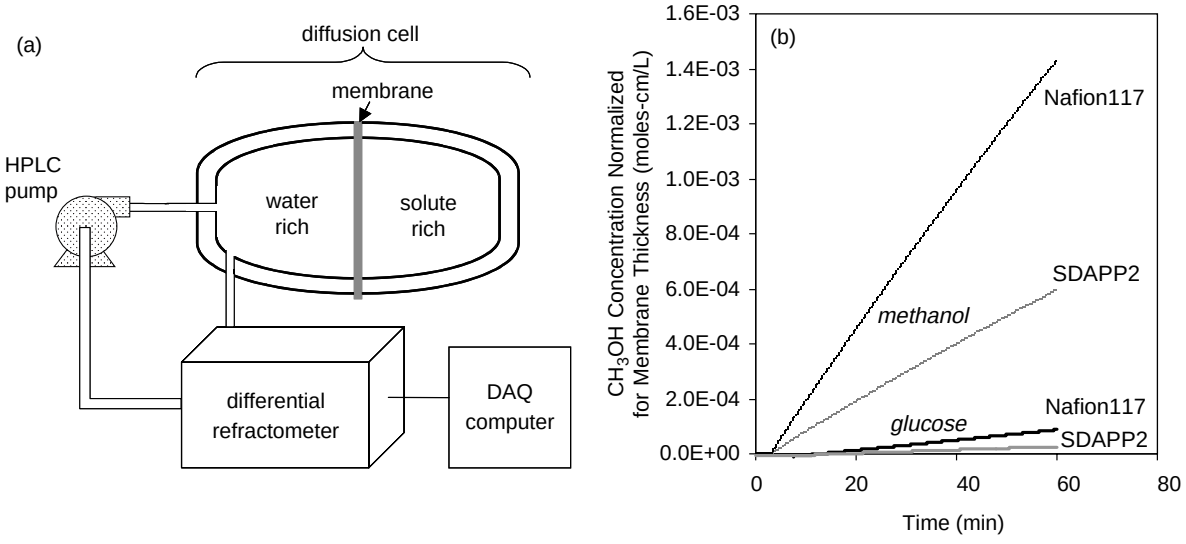


Fig. 1. (a) Membrane separated cell apparatus for measuring membrane methanol and glucose permeability, (b) thickness normalized concentration versus time plots for Nafion 117 and SDAPP2 during methanol and glucose permeation experiments.

A solute/water solution of a predefined concentration was introduced into one compartment of the cell while pure water filled the other compartment. The pure water compartment was then connected to a recirculation pump, a differential refractometer, and a data acquisition computer to conduct the measurement. Both compartments were vigorously stirred using submersible magnetic stirrers. Temperature was maintained by immersing the cell in a constant temperature water bath. Once both compartments were filled, the solute diffused from the solute rich compartment through the membrane into the water rich compartment, thus raising the concentration of the solute in the water compartment. The change in concentration of the solute in the water-rich compartment was measured by monitoring the refractive index of the solution. The permeability of the membrane was calculated from the rate of change of concentration for each side. The concentration (normalized for thickness) versus time data obtained in this experiment for two membranes (Nafion 117 and SDAPP2) during methanol and glucose permeation is shown in Fig. 1(b). The data indicates that N117 is much more permeable to both solutes than SDAPP2. This is explained further in the Section 2.

Cussler outlined the mathematical solution to the simple membrane separated cell first proposed by Barnes in 1934 and later simplified by Robinson and Stokes in 1960 [27]. This analysis assumes that the membrane reaches steady-state very quickly, there is no liquid mass transfer resistance, and it also neglects the water flux. The governing equations for this experiment are

$$-DH\chi t = \ln\left(\frac{c_{SR} - c_{WR}}{c^{o}_{SR} - c^{o}_{WR}}\right) \tag{3}$$

$$\chi = \frac{A}{l}\left(\frac{1}{V_L} + \frac{1}{V_R}\right) \tag{4}$$

where $DH$ is the permeability (the product of the diffusion coefficient and the solubility of the molecule of interest in the membrane), $c_{SR}$ and $c_{WR}$ are the concentration of solute in the solute-rich and water-rich compartments at time, $t$, with $c^{o}_{SR}$ and $c^{o}_{WR}$ being the initial concentration in the two compartments at time zero, $A$ is the active area of transport, $l$ is the thickness of the film, $V_L$ for the volume of the solute-rich cell, and $V_R$ for the water-rich volume at time $t$ equal to zero. The volumes of $V_L$ and $V_R$ are assumed to remain constant throughout the course of the experiment. A plot of $\ln[(c_{SR} - c_{WR})/(c^{o}_{SR} - c^{o}_{WR})]$ versus $t$ yields a straight line with slope $-DH\chi$. Once $\chi$ is determined by measuring the geometry of the cell and the membrane thickness, the permeability of the membrane can be calculated. The membrane thickness was determined after immersion in 18 MΩ water at 30 °C before the conductivity and permeability experiments. The swelling of the polymer membranes in liquid water at higher temperatures was not determined, however, this correction is estimated to be less than 5% as determined by stand-alone swelling measurements in liquid water at elevated, i.e. 80 °C, temperatures.

### 2.5. Dynamic scanning calorimetry

Fully hydrated membrane samples (about 15 mg total mass per sample) were blotted with a lab wipe to remove surface water then immediately placed into a DSC pan (O-ring model—TA Instruments) and sealed. The samples were then immediately placed in the calorimeter and cooled to −100 °C. The samples were held at −100 °C for 30 min then heated to 250 °C at a heating rate of 5 °C/min. The melting endotherms of the water contained in the membrane were integrated using the TA Universal Analysis software, and the heat of fusion for the water in the membranes was computed using

$$\Delta H_f = \frac{H}{m_{H_2O}} \tag{5}$$

where $\Delta H_f$ is the head of fusion for the water contained in the sample, $m_{H_2O}$ is the mass of water in the sample, and $H$ is the integrated energy from the melting endotherm.

### 2.6. Transmission electron microscopy

Membrane samples were soaked in a 2 M lead acetate solution in order to imbibe the hydrophilic domains with an electron dense species and contrast the hydrophilic regions from the hydrophobic regions of the polymer microstructure [28]. Lead acetate exchanged samples were dried by placing the samples between lab wipes under pressure for 48 h at ambient temperature. The dried samples were encapsulated in epoxy and then cross-sectioned in a microtome to yield 100 nm thick sections. The samples were imaged in a Hitachi 3300 TEM at two different magnifications. Lighter areas in the micrographs are associated with lead containing, hydrophilic domains.

## 3. Results and discussion

The proton conductivity of the SDAPP series and Nafion 117 was plotted versus hydration number in Fig. 2. For a given hydration number, the conductivity of Nafion is greater than SDAPP. This plot highlights the key difference between Nafion, a polyperfluorosulfonic acid membrane, and SDAPP, a sulfonated aromatic membrane. While SDAPP3 and Nafion have approximately the same number of water molecules per sulfonic acid group (Table 1), the difference between these two materials is due to the greater acidity of the perfluorosulfonic acid groups of Nafion and greater extent of phase separation resulting in higher conductivity for Nafion at a given hydration number [29]. The impact of these differences is that Nafion does not require as much absorbed water as SDAPP to achieve high proton conductivity. SDAPP membranes have greater proton conductivity than Nafion as the IEC is further increased, but this causes an increase in the hydration number and a corresponding large degree of swelling.

The proton conductivity of each sample was measured in liquid water at 30, 50, 70 and 80 °C. These results are plotted in Fig. 3 and used to calculate the activation energy for proton

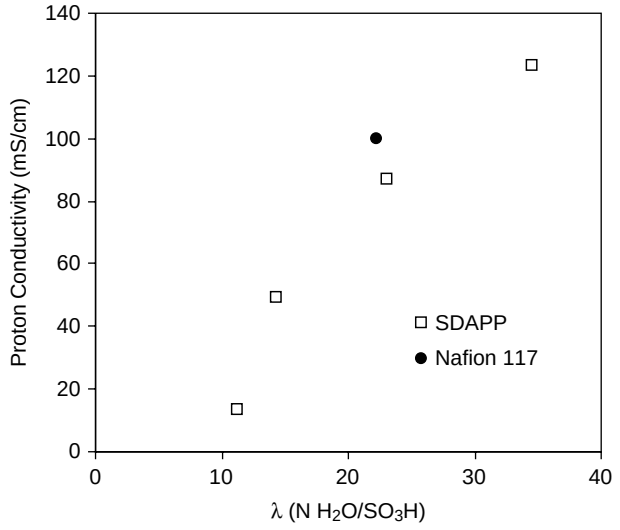


Fig. 2. Proton conductivity of SDAPP samples and Nafion 117 immersed in 30 °C liquid water as a function of hydration number.

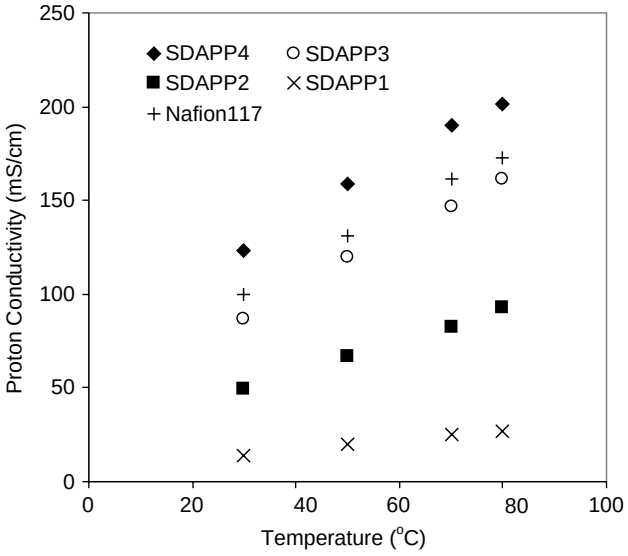


Fig. 3. Proton conductivity of SDAPP samples and Nafion 117 immersed in liquid water as a function of temperature.

conduction ($E_{a\sigma}$)—see Table 2. The proton conductivity of SDAPP membranes can be tuned to be greater than Nafion as in the case of SDAPP4, nearly equivalent to Nafion as in the case of SDAPP3, or less than Nafion for SDAPP1 and SDAPP2. The conductivity of all samples increased monotonically with temperature, albeit with different slopes. The $E_{a\sigma}$ of the samples followed a distinct trend with SDAPP1 having the highest activation energy, 3.0 kcal/mol, and SDAPP4 having the lowest value of 2.1 kcal/mol with Nafion falling in between SDAPP3 and SDAPP4. This trend mirrors that of proton conductivity for the samples. $E_{a\sigma}$ is a measure of how easily proton conduction occurs. Lower values of $E_{a\sigma}$ indicate that proton conductivity occurs readily and the barriers to proton conduction are low, whereas a high $E_{a\sigma}$ indicates that protons do not move as easily through the polymer.

We sought to further investigate this relationship between activation energy for transport in relation to the IEC of the membrane and ultimately the nature of water contained in the hydrated membrane by measuring the permeation of both methanol and glucose through the samples. The methanol permeability of the materials in this study is shown in Fig. 4. As with proton conductivity, the methanol permeability of SDAPP could be tuned to be greater than, equivalent to, or less than that of Nafion depending on the ion exchange capacity of the polymer. The activation energy for methanol permeability (Table 2) shows a similar trend to that of proton conductivity with SDAPP1 having the highest activation energy and SDAPP4 and Nafion having the lowest. This trend in activation energy for methanol permeability reiterates that transport occurs most easily in Nafion and SDAPP4 while transport is more difficult in SDAPP1, which is believed to be associated with the amount of water contained in the polymer and its state.

Proton conductivity and methanol or glucose permeability occur by different mechanisms. Proton conductivity relies on the presence of sulfonic acid groups and proton dissociation from these acid groups into the surrounding water in the hydrophilic regions of the polymer. The transport of protons is driven by an applied potential gradient. Methanol and glucose permeability occurs due to their respective concentration gradients across the membrane. However, the trends in transport of these two species and their activation energies give rise to a possible link between these two processes. It is proposed here that this link is the absorbed water in the membrane. Proton conductivity certainly occurs in the hydrophilic regions of the polymer where the sulfonic acid groups reside, and it is reasonable to surmise that the methanol/glucose transport is also occurring primarily in the hydrophilic regions as well. The permeability experiments

Table 1
IEC, water uptake, hydration number ($\lambda$), proton conductivity ($\sigma$), and adsorbed water heat of fusion ($\Delta H_f$) of SDAPP samples and Nafion 117

| | IEC (meq/g) | Water uptake (wt%) | $\lambda$ ($nH_2O/SO_3H$) | $\sigma$ (mS/cm) | $\Delta H_f$ (J/g) |
|---|---|---|---|---|---|
| SDAPP1 | 1.04 | 21 | 11.2 | 13 | 1.0 |
| SDAPP2 | 1.40 | 36 | 14.3 | 49 | 8.0 |
| SDAPP3 | 1.80 | 75 | 23.1 | 87 | 40 |
| SDAPP4 | 2.20 | 137 | 34.6 | 123 | 125 |
| Nafion 117 | 0.91 | 36 | 22.0 | 100 | 100 |

$\Delta H_f$ for bulk water is 334 J/g. Water uptake, $\lambda$, $\sigma$, and $\Delta H_f$ of SDAPP and Nafion 117 measured in liquid water at 30 °C.

Table 2
Activation energies for proton conduction ($E_{a\sigma}$), methanol permeability ($E_{aCH_3OH}$), and glucose permeability ($E_{aGLU}$) of SDAPP samples and Nafion 117

| | $E_{a\sigma}$ (kcal/mol) | ($E_{aCH_3OH}$) (kcal/mol) | $E_{aGLU}$ (kcal/mol) |
|---|---|---|---|
| SDAPP1 | 3.0 | 6.3 | 10.4 |
| SDAPP2 | 2.7 | 5.4 | 7.6 |
| SDAPP3 | 2.6 | 5.4 | 6.5 |
| SDAPP4 | 2.1 | 5.1 | 5.6 |
| Nafion 117 | 2.3 | 5.1 | 5.8 |

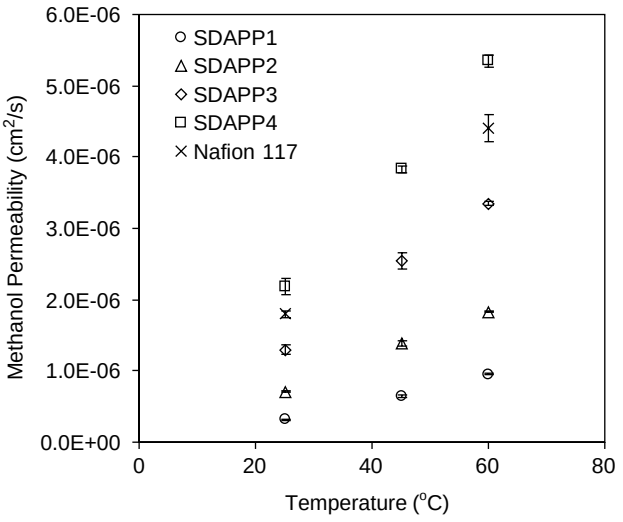


Fig. 4. Methanol permeability as a function of temperature for SDAPP samples and Nafion 117.

were performed with 1 M methanol on the methanol-rich side of the membrane. In this experiment, the membrane is primarily hydrated by water and the methanol plays a small role in hydration of the polymer structure. It is possible that the methanol is able to penetrate other parts of the polymer (the unsulfonated regions), but the unsulfonated SDAPP material does not sorb methanol, so it is reasonable to conclude that the large majority of the methanol transport is occurring in the water-filled hydrophilic domains.

The glucose permeability for all samples is plotted in Fig. 5. Glucose permeability was chosen because of the increasing interest in fuel cells powered by carbohydrate fuels, powdered by carbohydrate fuels [30]. Some bio fuel cells rely on membrane-less architectures, but in membrane-based cells, glucose crossover to the cathode could be a significant factor in performance degradation. Again the properties of Nafion can be bracketed by the SDAPP material depending on ion

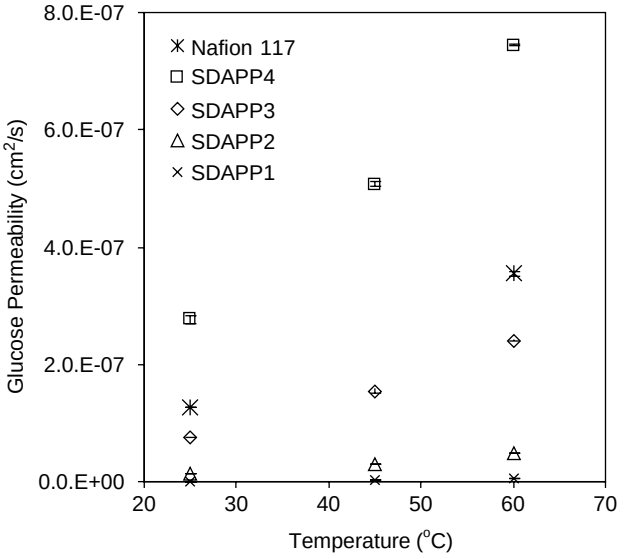


Fig. 5. Glucose permeability as a function of temperature for SDAPP samples and Nafion 117.

Table 3
Methanol and glucose permeability (DH) and relative selectivity (RS) at 30 °C of SDAPP samples and Nafion 117

| | Methanol DH ($cm^2/s$) | Glucose DH ($cm^2/s$) | Methanol RS | Glucose RS |
|---|---|---|---|---|
| SDAPP1 | $3.8\times10^{-7}$ | $1.2\times10^{-9}$ | 0.7 | 16.6 |
| SDAPP2 | $8.3\times10^{-7}$ | $1.6\times10^{-8}$ | 1.2 | 4.6 |
| SDAPP3 | $1.5\times10^{-6}$ | $9.1\times10^{-8}$ | 1.2 | 1.4 |
| SDAPP4 | $2.5\times10^{-6}$ | $3.2\times10^{-7}$ | 1.0 | 0.6 |
| Nafion 117 | $2.1\times10^{-6}$ | $1.5\times10^{-7}$ | 1.0 | 1.0 |

exchange capacity. Similar to proton conductivity and methanol permeability, the activation energy for glucose permeability (Table 2) follows the trend of SDAPP1 > SDAPP2 > SDAPP3 > Nafion 117 > SDAPP4, the order of which is mirrored in the absolute permeability numbers. A metric for selecting a high performance fuel cell membrane is its electrochemical selectivity [31]. The selectivity of a membrane is defined as the ratio of is proton conductivity and permeability

$$\beta = \frac{\sigma}{\mathrm{DH}} \tag{6}$$

where $\beta$ is the selectivity, $\sigma$ is the proton conductivity, and DH is the permeability. The relative selectivity (RS) is then the selectivity of the membrane divided by the selectivity of the control which in this case is Nafion 117

$$\mathrm{RS} = \frac{\beta_{\mathrm{m}}}{\beta_{\mathrm{Nafion}}}. \tag{7}$$

In this work we have computed the relative selectivity at 30 °C for the SDAPP membranes compared to Nafion 117 (Nafion's relative selectivity is 1) for both methanol and glucose and tabulated these values in Table 3. The relative selectivity of SDAPP membranes for glucose is much greater than the values for methanol and declines with increasing sulfonation. Comparing the selectivity of various molecules, such as methanol and glucose, can give an idea of how easily the molecules are transported through the hydrophilic regions

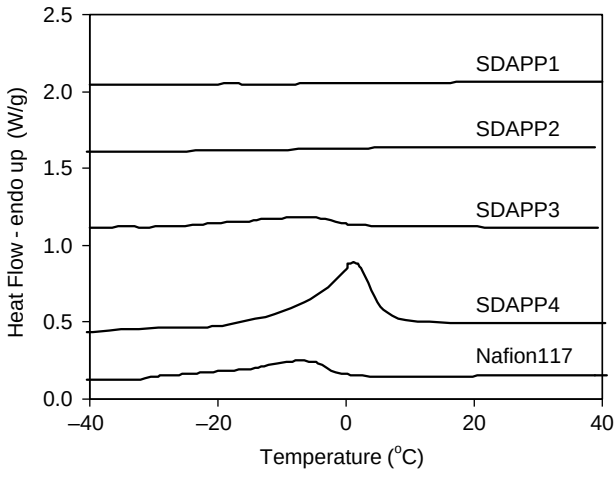


Fig. 6. DSC thermograms of adsorbed water melting endotherms for SDAPP samples and Nafion 117.

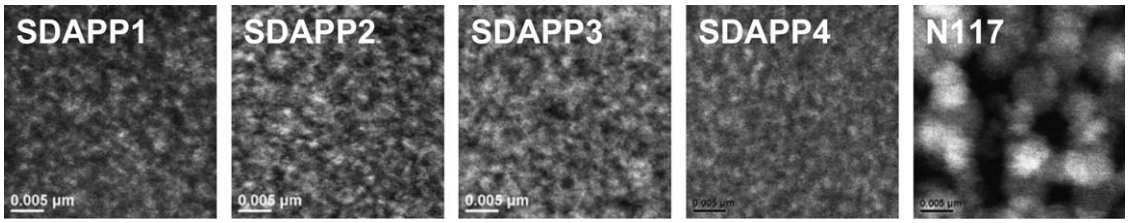


Fig. 7. Cross-sectional TEM micrographs of SDAPP samples and Nafion 117—high magnification.

of the membrane. High selectivity values for SDAPP1 and SDAPP2 mean that the small size of the hydrophilic regions of these membranes do not allow glucose to pass easily. For SDAPP3 and SDAPP4, the selectivity values of glucose and methanol approach one another. This seems to indicate that the hydrophilic regions of the swollen membranes are so large that they no longer impede transport of the larger glucose molecules and both methanol and glucose are easily transported across these membranes. A correction can be applied for the diffusion coefficients of methanol and glucose in water, but this correction is small compared to the sizable difference in permeabilities measured in this work.

Fig. 6 shows DSC traces of the fully hydrated membrane samples. The melting endotherms for the water contained in SDAPP 1 and SDAPP2 are not discernable at this scale, but there was enough departure from the baseline to integrate a very slight heat of fusion for the water in these samples. Endotherms for water in SDAPP3, SDAPP4, and Nafion are clearly distinguishable in the figure. Table 1 summarizes the differences in water uptake and the heat of fusion ($\Delta H_f$) for the water contained in Nafion versus the SDAPP series. The familiar order is again observed with SDAPP1 having the lowest value, and SDAPP4 having the highest value, with Nafion 117 falling in between SDAPP3 and SDAPP4. This set of data clearly demonstrates the role of the nature of water in these polymers and its effect on the membrane transport properties. SDAPP materials that contain primarily bound water as indicated by a low $\Delta H_f$ display suppressed transport properties while increasing the concentration of unbound water as observed by a larger $\Delta H_f$ results in greater transport.

An interesting comparison can be drawn between SDAPP2 and Nafion 117. Both of these materials have the same bulk water uptake at 36 wt%, but the $\Delta H_f$ for the water in SDAPP2 is much lower (8 J/g) compared to a value of 100 J/g as measured for Nafion 117. It is apparent that the water in SDAPP2 is more tightly bound within the polymer microstructure and has a lower concentration of unbound water than Nafion. Nafion does not bind water as tightly as SDAPP and therefore, shows greater transport properties on an ion exchange capacity basis than the SDAPP family of polymers. When compared on a water binding basis ($\Delta H_f$), Nafion falls in between SDAPP3 and SDAPP4, which is generally where its transport properties lie. This correlation is not perfect, but it is as useful model for comparing transport properties of different classes of proton exchange membranes.

Characterizing the morphology of proton exchange membranes, especially in the hydrated state, is notoriously difficult. Membranes imbibed with lead acetate and imaged with TEM in the dry state can provide some insight as to the ordering and relative sizes of the domains, but there is no way direct way to determine the size of the hydrated domains with this technique. The TEM images for the samples in this study are shown in Figs. 7 and 8 at two different magnifications. It is clear from these micrographs that some sort of phase separated domain structure exists within Nafion. Hydrophilic domains have an affinity for lead acetate and appear as white regions while the hydrophobic domains are black. The differences in morphology as observed by TEM invokes the concept of a highly phase separated material for Nafion where the sulfonic acid groups form clusters and undergo a certain level of self-assembly. However, the phase separation between hydrophilic and hydrophobic domains in SDAPP materials is not as distinct as in Nafion. There is a systematic increase in light-colored regions from SDAPP1 to SDAPP2 to SDAPP3, which is reasonable based on the increasing ion exchange capacity. SDAPP4 appears to be more uniform in nature than the other SDAPPs, which may represent a more evenly distributed volume fraction of hydrophilic and hydrophobic regions. Consequently, this higher concentration of hydrophilic domains, while improving conductivity and creating a more homogenous morphology, results in a material with high permeability and water uptake.

The TEM results support the transport and water melting endotherm studies. Smaller domains in SDAPP would give rise to more tightly bound water and lower transport properties until an ion exchange capacity is reached which creates a

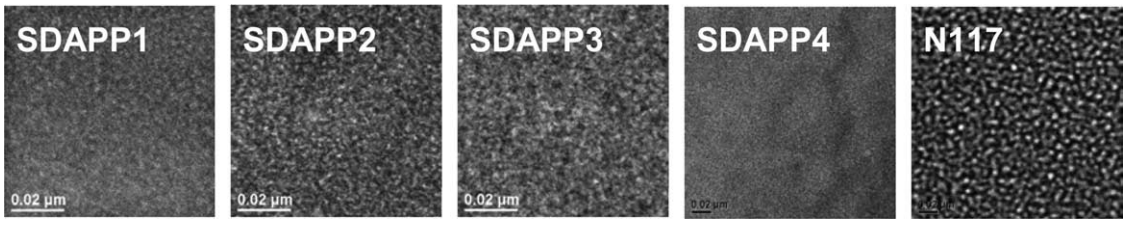


Fig. 8. Cross sectional TEM micrographs of SDAPP samples and Nafion 117—low magnification.

moderately swelling polymer (SDAPP3) with a significant portion of loosely bound water. Again, the TEM images only give a flavor of the size of the hydrophilic domains in the hydrated state but not the state of water within those hydrophilic domains.

## 4. Conclusions

In this work the transport of proton, methanol, and glucose was used as a probe of the morphology and nature of water in a series of sulfonated poly(phenylene)s versus Nafion 117. It was found that the transport of protons, methanol, and glucose all correlated well. In general, transport was lowest in SDAPP1 followed by SDAPP2, then SDAPP3, and Nafion 117 with SDAPP4 having the highest transport of the series. The opposite trend with minor variations was observed for the activation energy of the processes.

The nature of water in each membrane was probed with DSC, and the resulting heats of melting correlate well with the transport properties providing a direct link between the state of water binding in the samples and their respective transport properties. This would seem to indicate that the transport in these membranes is occurring through the hydrated regions with unbound or loosely bound water. Finally, the TEM images of each sample showed that the domains of the SDAPP family of polymers are smaller and not as well phase-separated as those in Nafion. The greater degree of self-assembly in Nafion into hydrophilic and hydrophobic domains due to greater polymer chain segmental mobility, highly fluorinated backbone, and greater acidity of groups produces an interesting balance between proton conductivity, nature of water, and observed fuel cell performance. Understanding these structure–property interrelationships is important for creating new membrane materials for methanol and other liquid-fed fuel cells.

## Acknowledgements

Ying-Bing Jian and Adrian Brearley from the University of New Mexico, Department of Earth and Planetary Sciences are gratefully acknowledged for their TEM sample preparation and imaging. Sandia National Laboratories is a multiprogram laboratory operated by Sandia Corporation, a Lockheed Martin Company, for the United States Department of Energy's National Nuclear Security Administration under contract DE-AC04-94AL85000.

## References

[1] Zheng J, Swager TM. Adv Polym Sci 2005;177:151.
[2] Aminabhavi TM, Toti US. Designed Monomers Polym 2003;6(3):211.
[3] Pandey P, Chauhan RS. Prog Polym Sci 2001;26(6):853.
[4] Ismail AF, Ridzuan N, Rahman SA. J Sci Technol 2002;24:1025.
[5] Bolto BA. Water Manage Purif Conservation Arid Climates 2000;2:227.
[6] Klinkmann H, Vienken J. Eur Dial Transplant Assoc-Eur Ren Assoc 1995;10(3):39.
[7] Johnson KM. Ind Water Treat 1996;28(6):24.
[8] Lonsdale HK. Future Trends Polym Sci Technol 1987;225.
[9] Burghoff HG, Pusch W. Polym Eng Sci 1980;20(4):305.
[10] Bromberg LE, Rudman AR, Vengerova NA, Eltsefon BS. Synth Polym Membr Proc Microsymp Macromol 1987;29:397.
[11] Yasuda H, Olf HG, Crist B, Lamaze CE, Peterlin A. Water Struct Water Polym Interface Proc Symp 1972;39.
[12] Pusch W. Desalination 1990;77:35.
[13] Laporta M, Pegoraro M, Zanderighi L. Phys Chem Chem Phys 1999; 1(19):4619.
[14] Hodge RM, Bastow TJ, Edward GH, Simon GP, Hill AJ. Macromolecules 1996;29(25):8137.
[15] Burghoff HG, Pusch W. Polym Eng Sci 1980;20(4):305.
[16] Hubbell WH, Brandt H, Munir ZAJ. Appl Polym Sci Polym Phys Ed 1975;13(3):493.
[17] Sivashinsky N, Tanny GB. J Appl Polym Sci 1981;26(8):2625.
[18] Fushimi H, Ando I, Iijima T. Polymer 1991;32(2):241.
[19] Ostrovskii D, Paronen M, Sundholm F, Torell LM. Solid State Ionics 1999;116(3,4):301.
[20] Kim YS, Dong L, Hickner MA, Glass TE, Webb V, McGrath JE. Macromolecules 2003;36(17):6281.
[21] Rajendran RG. MRS Bull 2005;30(8):587.
[22] Hickner MA, Ghassemi H, Kim YS, Einsla BR, McGrath JE. Chem Rev 2004;104(10):4587.
[23] Rikukawa M, Sanui K. Prog Polym Sci 2000;25(10):1463.
[24] Fujimoto CH, Hickner MA, Cornelius CJ, Loy DA. Macromolecules 2005;38(12):5010.
[25] Zawodzinski TA, Deroin C, Radzinski S, Sherman J, Smith VT, Springer TE, et al. J Electrochem Soc 1993;140:1041.
[26] Yin Y, Fang J, Cui Y, Tanaka K, Kita H, Okamoto KI. Polymer 2003; 44(16):4509.
[27] Cussler EL.. 2nd ed Diffusion mass transfer in fluid systems. New York: Cambridge University Press; 1997.
[28] Ding J, Chuy C, Holdcroft S. Chem Mat 2001;13(7):2231.
[29] Hickner MA, Pivovar BS. Fuel Cells 2005;5(2):213.
[30] Barton SC, Gallaway J, Atanassov P. Chem Rev 2004;104:4867.
[31] Pivovar BS, Wang Y, Cussler EL. J Membr Sci 1999;154:155.